Thorium(IV) and Uranium(IV) Thioether and Selenoether Complexes: Synthesis and An–ER_2 (E = S, Se) Bonding Comparison

Novan A. G. Gray and David J. H. Emslie*

Department of Chemistry and Chemical Biology, McMaster University, Hamilton, Ontario L8S 4M1, Canada

Supporting Information Placeholder

ABSTRACT: Reactions of the rigid thioether- and selenoether-containing ligand salts [{Li(AE_2^{Ph2})}$_2$] (E = S or Se; AE_2^{Ph2} = 4,5-bis(phenylchalcogenido)-2,7,9,9-tetramethylacridanide) with $ThCl_4(dme)_2$ or UCl_4 (for E = Se) afforded the actinide chalcogenoether complexes [(AE_2^{Ph2})$_2$$ThCl_2$] (E = S (**1**), Se (**2**)) and [(ASe_2^{Ph2})$_2$$UCl_2$] (**3**). X-ray crystal structures of **1**–**3** revealed tetravalent actinide cations complexed to two κ^3-coordinated AE_2^{Ph2} ligands, with Th–ER_2 and U–ER_2 distances below the sum of the covalent radii. Complexes **1**–**3** provide extremely rare examples of thorium–thioether, thorium–selenoether, and uranium–selenoether bonds, and **1** and **2** contain the shortest known Th–SR_2 and Th–SeR_2 distances. DFT and QTAIM calculations confirm the presence of significant An(IV)–ER_2 interactions in **1**–**3** and provide insight into the extent of covalency in the An–ER_2 bonds.

INTRODUCTION

Sulfur-donor ligands such as dithiophosphinates ($R_2PS_2^-$) have been shown to be particularly effective for selective actinide complexation, as required in nuclear fuel reprocessing.[1-6] This selectivity is thought to arise, in part, from increased covalency in bonding with the early/mid actinides relative to the lanthanides, stemming from the greater radial extension of the actinide 5*f* orbitals relative to the lanthanide 4*f* orbitals[7] combined with the increased polarizability and lower electronegativity of soft donor atoms. However, many questions remain regarding the extent to which the character of actinide–soft donor interactions is affected by the identity and oxidation state of the actinide metal, as well as the nature of the soft donor and co-ligands.

A substantial number of actinide complexes bearing anionic chalcogen donors, such as thiolates and sulfides, have been reported.[8] Additionally, a smaller number of actinide complexes have been prepared bearing ligands, such as dichalcogenophosphinates ($R_2PE_2^-$; E = S, Se)[9-12] and imidodiphosphinochalcogenides ($N(PR_2E)_2^-$; E = S, Se, Te),[13-17] with at least one resonance structure that features a neutral chalcogen donor, and others that place a negative charge on the chalcogen atom. By contrast, actinide complexes bearing neutral L-type chalcogen donors such as chalcogenoethers are scarce, especially for the heavier chalcogens (*vide infra*), despite the potential for a reduced ionic component to bonding.

At the time of writing, there are only 13 complexes containing uranium–thioether (SR_2) interactions in the Cambridge Structural Database.† Complexes featuring monodentate thioether ligands are [(^{Me}Cp)$_3$U(tht)][18] and [{(κ^3-$MeBH_3$)$_4$U(μ-tht)}$_2$],[19] in which the tetrahydrothiophene (tht) ligand is terminal or bridging, respectively. Uranium complexes bearing chelating thioether ligands are the 1,2-bis(methylthio)ethane complex [(κ^3-$MeBH_3$)$_4$U(κ^2-$MeSCH_2CH_2SMe$)][20] and the thiacrown complexes [UI_3(κ^3-9S3)($MeCN$)$_2$] (9S3 = (SCH_2CH_2)$_3$)[21] and [(κ^3-BH_4)$_2$U(κ^6-18S6)][BPh_4] (18S6 = (SCH_2CH_2)$_6$).[22] All other examples employ more elaborate ligands containing one or more thioether in combination with N- and/or O- donors.[23-29] Structurally characterized thioether complexes of actinides other than uranium are limited to the thorium and plutonium compounds [Cp*Th(κ^6-{B_3(*o*-$O_2C_6H_4$)$_6$})(SMe_2)][30] and [PuI_3(κ^3-9-ane-S_3)($MeCN$)$_2$].[31]

In 2015, Walensky and co-workers reported the thorium(IV) complex [{(4,6-^{t}Bu$_2$$C_6H_2O$)$_2$Se}$_2$Th($THF$)$_2$] which contains two dianionic selenoether-containing ligands. The authors concluded that although the Th–Se distances (3.2306(5) and 3.3262(5) Å) lie outside of the sum of the effective ionic radii, a significant difference between the ^{77}Se NMR resonance of the complex versus the protonated ligand points to the existence of Th–SeR_2 dative interactions.[32] Uranium and neptunium analogues of this complex were subsequently reported by Lukens and Walensky *et al.*, with An–SeR_2 distances of 3.1642(6) and 3.2606(6) Å (U) or 3.1289(15) and 3.2287(17) Å (Np). However, the authors concluded an absence of An–SeR_2 interactions based on An–Se distances outside of the sum of Pyykkö's covalent radii.[33] Uranium complexes containing a bridging Se_4^{2-} ligand have also been reported, and dative interactions were proposed between uranium and the central selenium atoms in the Se_4 chain (U–$Se_{central}$ 3.001(1)–3.178(1) Å).[34,35]

Recently, we reported the use of rigid ligands containing two thioether or selenoether donors flanking a central amido anion, AE_2^{Ph2} (E = S, Se; AE_2^{Ph2} = 4,5-bis(phenylchalcogenido)-2,7,9,9-tetramethylacridanide), for the synthesis of the uranium(IV) chalcogenoether complexes [(AE_2^{Ph2})$_2$$UI_2$] (E = S, Se). These complexes provided uncommon examples of U–SR_2 bonds and the first reported U–SeR_2 interactions.[28] Quantum chemical calculations and trends in crystallographic U–E distances (adjusted for differences in the covalent radii of S and Se) revealed increased covalency in the U–SeR_2 versus the U–SR_2 interactions.

Herein, we report the synthesis of the first thorium AE_2^{Ph2} complexes, [(AE_2^{Ph2})$_2$$ThCl_2$] (E = S, Se), and for comparison, a direct uranium(IV) dichloro analogue of the thorium selenoether complex, [(ASe_2^{Ph2})$_2$$UCl_2$]. Crystallographic and computational analysis of actinide–chalcogenoether bonding in these complexes is described.

RESULTS AND DISCUSSION

Reaction of one equivalent of [{Li(AS_2^{Ph2})}$_2$] or [{Li(ASe_2^{Ph2})}$_2$] with $ThCl_4(dme)_2$ in toluene afforded [(AS_2^{Ph2})$_2$$ThCl_2$] (**1**) and [($ASe_2^{Ph2}$)$_2$$ThCl_2$] (**2**) as orange solids in 29 and 40 % yield,

respectively.[§] The dark brown uranium analogue $[(ASe_2^{Ph2})_2UCl_2]$ (**3**) was generated similarly via the reaction of one equivalent of $[\{Li(ASe_2^{Ph2})\}_2]$ with UCl_4 in THF, and was isolated in 33 % yield (Scheme 1).[§]

Room temperature ^{1}H NMR spectra for diamagnetic **1** and **2** in C_6D_6 each display a comparable set of four methyl and ten aryl signals, and the ^{77}Se{^{1}H} NMR spectrum of **2** contains two singlets at 392.78 and 347.96 ppm (for comparison, the ^{77}Se chemical shifts of $H(ASe_2^{Ph2})$, $[\{Li(ASe_2^{Ph2})\}_2]$ and $[K(ASe_2^{Ph2})(dme)_2]$ are 295.39, 283.43 and 357.02 ppm, respectively).[36] These data are consistent with equivalent AE_2^{Ph2} (E = S or Se) ligands with top-bottom and side-to-side asymmetry. However, most of the ^{1}H NMR resonances for **1** are broader than those of **2**, suggestive of fluxional processes in solution. At low temperature (Figure S4), the ^{1}H NMR signals for **1** sharpened, whereas at high temperature (381 K; Figure S3) several pairs of signals (Ar*Me*, $CH^{1/8}$, $CH^{3/6}$ and *m*/*p*-C_6H_5, but not CMe_2) broadened and coalesced to a single peak, indicative of a fluxional process which removes side-to-side asymmetry but not top-bottom asymmetry.

The ^{1}H NMR spectrum of the uranium–selenoether complex (**3**) exhibits fourteen (4 x 6H, 4 x 4H, 6 x 2H) paramagnetically shifted resonances between –15 ppm and +25 ppm, again consistent with equivalent ligands lacking top-bottom and side-to-side symmetry. A comparable set of signals was previously reported for the uranium(IV) iodo complexes $[(AS_2^{Ph2})_2UI_2]$ and $[(ASe_2^{Ph2})_2UI_2]$.[28]

Scheme 1. Synthesis of actinide complexes **1**–**3**.

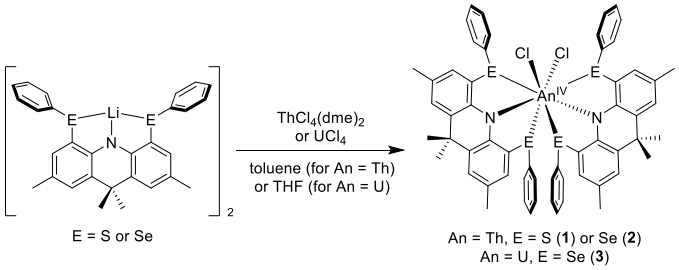

X-ray quality crystals of the thorium complexes **1**·2 hexanes and **2**·toluene (Figure 1) and the uranium complex **3**·toluene (Figure 2) were obtained from *o*-difluorobenzene/hexanes (for **1**) or toluene/hexanes (for **2** and **3**) at –30 °C. Selenoether complexes **2** and **3** are isostructural and isomorphous in the solid state, crystallizing in the centrosymmetric monoclinic space group C_2/c. By contrast, the thorium thioether complex **1** crystallized in the orthorhombic space group *Pbca*. All three compounds feature two κ^3-coordinated ligands with the halide co-ligands *cis* to one another, as observed in the previously reported uranium(IV) iodo complexes $[(AS_2^{Ph2})_2UI_2]$ and $[(ASe_2^{Ph2})_2UI_2]$.[28] The coordination geometry in **1** and **3** is best described as distorted triangular dodecahedral, whereas that in **2** is distorted biaugmented trigonal prismatic, according to SHAPE analysis (Figure S14).

The solid-state structures of the thioether and selenoether complexes differ significantly in the position of the phenyl substituents on the chalcogen donors. In compound **1**, the phenyl rings in each ligand are positioned on the same side of the ligand backbone (relative to the plane of the ligand backbone), potentially allowing for intra-ligand π-stacking between the phenyl rings on S(1) and S(2), and on S(3) and S(4). By contrast, in **2** and **3**, the phenyl rings in each ligand are positioned on opposite sides of the ligand backbone, possibly allowing for in inter-ligand π-stacking between the phenyl rings on Se(1) and Se(1').[‡]

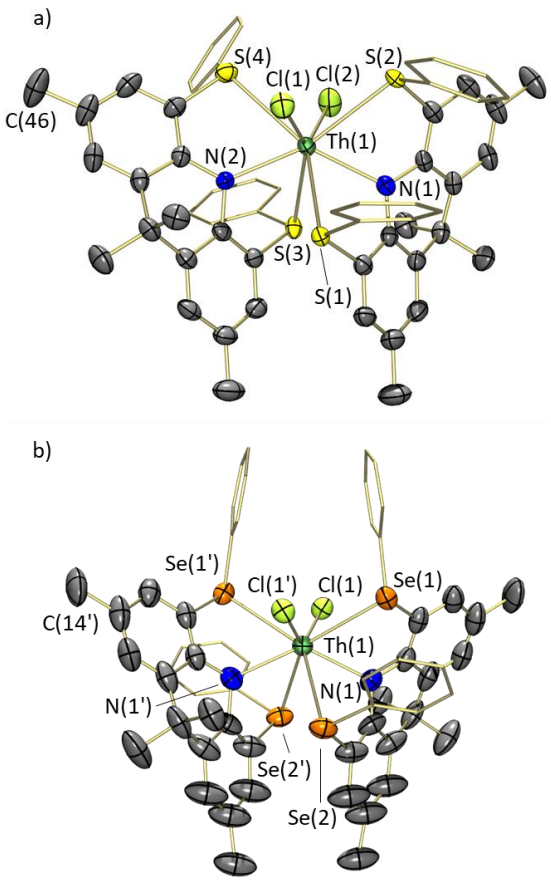

Figure 1. X-ray crystal structures of a) $[(AS_2^{Ph2})_2ThCl_2]$ ·2 hexanes (**1**·2 hexanes) and b) $[(ASe_2^{Ph2})_2ThCl_2]$·toluene (**2**·toluene). Lattice solvent in **1**·2 hexanes was badly disordered and was therefore treated with the BYPASS method.[37] Hydrogen atoms and lattice solvent in **2**·toluene are omitted, and phenyl substituents are presented in wireframe for clarity. Ellipsoids are shown at 75 % (**1**·2 hexanes) and 50 % (**2**·toluene) probability**.**

The Th–S distances in **1** are 3.033(1)–3.076(1) Å, which lie within the sum of the covalent radii of thorium and sulfur (3.11 Å)[38] and are slightly shorter (by 0.013–0.056 Å) than those in the previously reported crystallographically characterized thorium thioether complex, $[Cp^*Th(\kappa^6\text{-}\{B_3(o\text{-}O_2C_6H_4)_6\})(SMe_2)]$ (3.089(1) Å),[30] although it should be noted that crystal packing can have a particularly significant impact on weak bonds with shallow potential energy surfaces. Both AS_2^{Ph2} ligands have one longer and one shorter Th–S distance; the shorter distance (Th–S(1) and Th–S(3)) is approximately *trans* to a chloride ligand, while the longer distance (Th–S(2) and Th–S(4)) is approximately *trans* to the amido donor. The Th–Se distances in **2** are 3.1477(9) and 3.1707(8) Å, which also lie within the sum of the covalent radii (3.26 Å),[38] and for each ligand the longer Th–Se distance (Th–Se(2)) is *trans* to chloride. The Th–Se distances in **2** are significantly shorter than those in $[\{(4,6\text{-}^tBu_2C_6H_2O)_2Se\}_2Th(THF)_2]$ (3.2306(5) Å and 3.3262(5) Å).[32] The average Th–Se distance in **2** is 0.106(1) Å longer than the average Th–S distance in **1** , which is less than the difference in the covalent radii of S versus Se. (0.15 Å),[38] potentially indicative of stronger Th–ER_2 bonding in the selenoether complex. The Th–N distances in **1** and **2** are similar to one another at 2.424(2)–2.440(2) Å and 2.440(5) Å, respectively, and the Th–Cl distances in **1** and **2** are 2.637(1)–2.668(1) Å and 2.666(1) Å, respectively. The geometries at sulfur and selenium in **1** and **2** are pyramidal with the sum of the C–E–C and U–E–C angles (E = S or Se) ranging from 306.8(2)° to 318.8(2)° in **1** and 289.8(4)° to 302.7(3)° in **2**. The ligand backbones are bent by 21° and 32° in **1**,

and 26° in **2**, and thorium is located 1.81–1.85 Å and 2.10 Å out of the plane of the SNS and SeNSe donors, respectively.

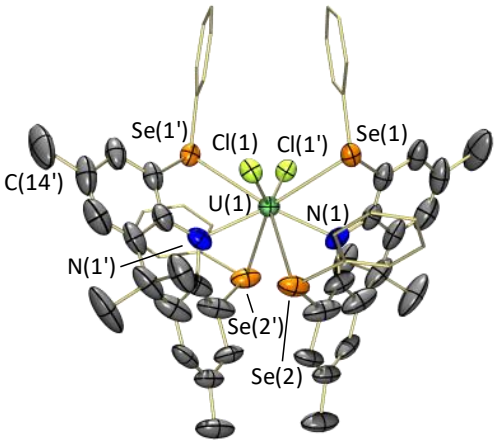

Figure 2. X-ray crystal structure of $[(ASe_2^{Ph2})_2UCl_2]$·toluene (**3**·toluene). Only the dominant component of a two-part (62:38) disorder affecting one of the aryl rings of the acridanide ligand backbone is shown. Lattice solvent and hydrogen atoms are omitted, and phenyl substituents are presented in wireframe for clarity. Ellipsoids are shown at 50 % probability.

The solid-state structure of uranium complex **3** features U–Se distances of 3.0886(8) and 3.1128(8) Å, and as in **2**, the longer An–E distance (U–Se(2)) is *trans* to chloride. The U–Se distances in **3** are longer than those in the uranium(IV) iodo complex $[(ASe_2^{Ph2})_2UI_2]$ (3.049(1) and 3.067(1) Å),[28] but remain well within the sum of the covalent radii of uranium and selenium (3.16 Å).[38] The average U–Se distance in **3** is 0.059(1) Å shorter than that in the thorium analogue (**2**), which is slightly greater than the difference in the 8-coordinate ionic radii for Th(IV) and U(IV) (0.05 Å).[39] The U–N distance in **3** is 2.375(5) Å, which is statistically equivalent to that in $[(ASe_2^{Ph2})_2UI_2]$ (2.378(9) Å),[28] and the U–Cl distance is 2.619(1) Å. The selenium atoms in **3** are pyramidal, with the sum of the C–Se–C and U–Se–C angles equal to 291.8(6)° and 304.2(3)° in the dominant component of a two-part disorder (62:38; affecting one of the aryl rings of the acridanide ligand backbone), and 289.8(6)° and 291(1)° in the minor component. Uranium is located 2.03 Å out of the SeNSe-donor plane, and the ligand is bent by 26° in the major disorder component and 36° in the minor component.

DFT (ADF/AMS, gas-phase, all-electron, PBE, D3-BJ, TZ2P, ZORA; spin-restricted for **1**–**2**; spin-unrestricted with a net spin polarization of 2 for **3**) and QTAIM calculations were employed to gain insight into the nature of actinide–chalcogenoether bonding in **1**-**3**. The geometry optimized structures are in good agreement with the X-ray crystal structures, with calculated An–Cl, An–N and An–E distances within 0.02, 0.05 and 0.05 Å of the experimental values, respectively (Table S2-S3). The three compounds feature (a) average An–E Mayer bond orders of 0.42–0.44, (b) QTAIM bond delocalization indices, δ, of 0.27–0.33, (c) average values for the total energy density of Cremer and Kraka at the bond critical point (H_b; positive values are indicative of negligible covalency)[40,41] ranging from -5.1×10^{-3} a.u. to -5.8×10^{-3} a.u., and (d) average actinide atomic orbital contributions to the NLMOs for An–E bonding pairs (An %; normalized to include only An and E contributions) of 9.8–14.7 %, all of which are indicative of significant and partially covalent An–ER_2 interactions; see Table 1. These values contrast those for the M–ER_2 interactions in recently reported lithium and potassium complexes of the AS_2^{Ph2} and ASe_2^{Ph2} ligands: Mayer bond orders below 0.13 (K) or 0.29 (Li), δ values below 0.1, positive H_b values, and alkali metal atomic orbital contributions to the NLMOs for M–E (M = Li, K) bonding pairs below 0.5 % (K) or 2.7 % (Li).[36]

The δ, H_b and An % values for Th–SR_2 bonding in **1** versus Th–SeR_2 bonding in **2** (Table 1) are suggestive of slightly increased covalency in the latter compound, consistent with the experimentally observed Th–E bond lengths which differ by less than the difference in the covalent radii of S and Se (*vide supra*). It is also notable that most computational metrics (δ, An %, Mayer bond order) point to increased covalency in the U–Se bonds in **3** compared with the Th–Se bonds in **2**, consistent with trends observed in studies of An–Se bonding in U and Th diseleno-phosphinate and -phosphonate complexes.[9,10,11] The Hirshfeld charge on the metal center in thioether complex **1** is 0.401, compared with 0.376, and 0.379 in selenoether complexes **2** and **3**, respectively. These data are also consistent with increased covalency in the selenoether complexes.

In **1**–**3**, the metal orbitals that contribute to the An–E bonding pair NLMOs are primarily of 5*f*-, 6*d*- and 7*s*-character, with negligible 7*p*-orbital involvement. For thorium complex (**1**), the average metal orbital participation follows the order *d* > *f* > *s* (50.3 % *d*, 32.3 % *f*, 17.3 % *s*). Relative to compound **1**, the percentage of *d*-orbital participation in the selenoether analogue (**2**) is reduced and the *s*-orbital contribution is increased (43.1 % *d*, 32.3 % *f*, 24.5 % *s*), whereas in the uranium selenoether complex (**3**), the percentage of *d*-orbital participation is reduced and *f*-orbital involvement is increased (40.9 % *d*, 42.8 % *f*, 16.3 % *s*). The relative metal orbital contributions for the iodo analogue $[(ASe_2^{Ph2})_2UI_2]$ are similar (36.8 % *d*, 45.8 % *f*, 17.3 % *s*)[28] to those for compound **3**, albeit with slightly increased *f*-orbital and decreased *d*-orbital participation. However, An % (the average actinide atomic orbital contributions to the NLMOs for U–E bonding pairs, normalized to include only An and E contributions) is higher in the iodo compound, and in fact, all metrics for An–E bond covalency in Table 1 point to increased covalency in the U–SeR_2 bonds of $[(ASe_2^{Ph2})_2UI_2]$ versus **3**. The reason for this is unclear, but it may stem from a significantly lower Hirshfeld charge on uranium in the iodo compound (0.320)[28] resulting from the lower electronegativity of iodine versus chlorine.

SUMMARY AND CONCLUSIONS

Rigid 4,5-bis(phenylchalcogenido)-2,7,9,9-tetramethylacridanide anions, AS_2^{Ph2} and ASe_2^{Ph2}, have been used to access the thorium(IV) thio- and seleno-ether complexes $[(AE_2^{Ph2})_2ThCl_2]$ (E = S (**1**) and Se (**2**)) and the uranium(IV)-selenoether analogue $[(ASe_2^{Ph2})_2UCl_2]$ (**3**). In the solid-state structures of **1**–**3**, the tetravalent actinide cations are κ^3-coordinated to two AE_2^{Ph2} ligands, with Th–ER_2 and U–ER_2 distances below the sum of the covalent radii. Complexes **1**-**3** provide extremely rare examples of Th–SR_2, Th–SeR_2 and U–SeR_2 interactions, and **1** and **2** contain the shortest known Th–SR_2 and Th–SeR_2 distances. DFT and QTAIM calculations confirm the presence of significant and partially covalent An(IV)–ER_2 interactions in **1**–**3**, with increased covalency in the U–SeR_2 versus Th–SeR_2 interactions, and slightly increased covalency in the Th–SeR_2 versus Th–SR_2 bonds. Crystallographically determined bond lengths and DFT calculations also indicate lower covalency in the U–SeR_2 bonds in **3** relative to the previously reported iodo analogue, $[(ASe_2^{Ph2})_2UI_2]$, illustrating the impact of co-ligands on bonding. These findings provide insight into the bonding between actinide cations and soft neutral donors, with potential relevance to the development of improved ligands for selective actinide complexation in nuclear fuel reprocessing.

Table 1. Selected computational data for compounds **1**–**3** and previously reported $[(AS_2^{Ph2})_2UI_2]$ and $[(ASe_2^{Ph2})_2UI_2]$:[28] Hirshfeld charge, QTAIM bond delocalization index (δ) and the total energy density of Cremer and Kraka at the bond critical point (H_b), percent contribution of actinide atomic orbitals to NLMOs for An–E bonding pairs (normalized to include only An and E contributions), and Mayer bond orders; An = Th or U; E = S or Se; X = Cl or I.

Compound	Hirshfeld Charge at Th or U	Avg. δ (An–E)	Avg. H_b (a.u) (An–E)	Avg. % An in An–E NLMOs	Avg. An–E Mayer bond order	Avg. An–X Mayer bond order	Avg. An–N Mayer bond order
$[(AS_2^{Ph2})_2ThCl_2]$ (**1**)	0.401	0.272	-5.1×10^{-3}	9.8–10.0	0.42	1.04	0.45
$[(ASe_2^{Ph2})_2ThCl_2]$ (**2**)	0.376	0.292	-5.8×10^{-3}	9.9–10.6	0.42	1.04	0.44
$[(ASe_2^{Ph2})_2UCl_2]$ (**3**)	0.379	0.326	-5.6×10^{-3}	11.4–14.7[a]	0.44	1.05	0.52
$[(AS_2^{Ph2})_2UI_2]$[28]	0.353	0.329	-6.0×10^{-3}	10.7–12.8[a]	0.48	0.94	0.53
$[(ASe_2^{Ph2})_2UI_2]$[28]	0.320	0.362	-7.1×10^{-3}	12.5–15.8[a]	0.48	0.90	0.56

[a] range includes α and β spin NLMOs.

EXPERIMENTAL SECTION

General Details: An argon-filled MBraun UNIlab glovebox equipped with a −30 °C freezer was employed for the manipulation and storage of all oxygen- and moisture-sensitive compounds. Air-sensitive reactions were performed on a double-manifold vacuum line equipped with an Edwards RV 12 vacuum pump using standard techniques. The vacuum was measured periodically using a Kurt J. Lesker 275i convection enhanced Pirani gauge and was always between 5 and 10 mTorr. $ThCl_4(dme)_2$,[42] UCl_4,[43] $[\{Li(AS_2^{Ph2})\}_2]$[36] and $[\{Li(ASe_2^{Ph2})\}_2]$[36] were synthesized following previously reported procedures. ***Caution!*** *Natural abundance thorium (primary isotope ^{232}Th) and uranium (99.3% ^{238}U; 0.7 % ^{235}U) are α-emitters with long half-lives (1.41 × 10^{10} years for ^{232}Th, 4.47 × 10^9 years for ^{238}U, and 7.04 x 10^8 years for ^{235}U), and other elements in the decay chains for these elements are α- or β-emitters, and in some cases also γ-emitters. Manipulations and reactions should be carried out in fume hoods or in an inert atmosphere glovebox in a laboratory equipped with appropriate monitoring equipment.*

Benzene was purchased from Sigma Aldrich. Hexanes, toluene, Et_2O, and THF were purchased from Caledon, *o*-difluorobenzene was purchased from Oakwood, and deuterated solvents were purchased from Cambridge Isotope Laboratories, Inc. Hexanes, Et_2O, THF, and toluene were initially dried and distilled at atmospheric pressure from sodium/benzophenone (hexanes, Et_2O, THF) and sodium (toluene). *o*-difluorobenzene and benzene were dried by stirring over 4 Å molecular sieves for 1 week, degassing, and distilling under reduced pressure. All solvents were stored over an appropriate drying agent (Et_2O, toluene, benzene, THF, C_6D_6, toluene-d_8 = Na/Ph_2CO; hexanes = Na/Ph_2CO/tetraglyme) and introduced to reactions or air-free solvent storage flasks via vacuum transfer with condensation at −78 °C or inside of an argon-filled glovebox. Argon gas was purchased from Air Liquide.

^1H, $^{13}C\{^1H\}$ and $^{77}Se\{^1H\}$ NMR spectra of all air-sensitive samples were acquired at room temperature in J-Young tubes on either a Bruker AV-600 or AV-500 MHz spectrometer. ^1H and $^{13}C\{^1H\}$ spectra were referenced relative to the residual proteo signals of the solvent (C_6D_6 or toluene-d_8) or the solvent carbon resonances, respectively (C_6D_6: ^1H = 7.16 ppm; ^{13}C = 128.06 ppm/toluene-*d*8: ^1H = 7.09, 7.01, 6.97, 2.08 ppm; ^{13}C = 137.48, 128.87, 127.96, 125.13, 20.43 ppm). $^{77}Se\{^1H\}$ spectra were referenced by indirect referencing[44] from a ^1H NMR spectrum. Peak assignments in the spectra of all new compounds were made with the aid of DEPT-q, COSY, HSQC, and HMBC experiments. All $^{13}C\{^1H\}$ signals are singlets unless otherwise specified.

X-ray crystallographic analyses were performed with suitable crystals coated in paratone oil on either a STOE IPDS II diffractometer equipped with a 3 kW sealed tube Mo generator or a Bruker Dual Source D8 Venture diffractometer using the IμS 3.0 Mo source at 70 W with a HELIOS Mo focusing optic (ELM33) in the McMaster Analytical X-ray (MAX) Diffraction Facility. Raw data was processed using XPREP (as part of the APEX v4 software) and solved by intrinsic (SHELXT)[45] methods. Structure refinement was performed with SHELXL[46] in OLEX 2.[47] In the structure of **1**·2 hexanes, hexane solvent molecules were badly disordered and could not be satisfactorily modelled and were therefore treated with the BYPASS method.[37] Images were rendered using Ortep3 and POV-Ray. Images were rendered using Ortep3 and POV-Ray.

Combustion elemental analyses were carried out at McMaster University.

Geometry optimization calculations were conducted with ADF within the AMS DFT package (SCM, version 2021.104, 2022.103 or 2023.102).[48-50] Calculations were performed in the gas phase within the generalized gradient approximation using the 1996 Perdew−Burke−Ernzerhof exchange and correlation functional (PBE),[51] using the scalar zeroth-order regular approximation (ZORA)[52-56] for relativistic effects, and Grimme's DFT-D3-BJ dispersion correction.[57,58] These calculations were conducted using all-electron triple-ζ basis sets with two polarization functions (TZ2P), and fine integration grids (Becke[59,60] very good quality) with default convergence criteria for energy and gradients. All uranium calculations were performed with the UNRESTRICTED command and a spin polarization of 2. Analytical frequency calculations[61-63] were performed to ensure that each geometry optimization led to an energy minimum. Quantum theory of atoms in molecules (QTAIM)[64] properties were obtained using the QTAIM keyword with an analysis level of Full,[65-72] and NBO[73] analysis was carried out using NBO 6.0 within the AMS DFT package.

$[(AS_2^{Ph2})_2ThCl_2]$ (1): In the glovebox, $ThCl_4(dme)_2$ (80.0 mg, 0.144 mmol) and $[\{Li(AS_2^{Ph2})\}_2]$ (133 mg, 0.289 mmol) were charged to a 20 mL scintillation vial, dissolved in ~ 5 mL of toluene and stirred for 20 minutes. The orange solution was filtered through a small celite plug to remove LiCl and collected in a 25 mL round-bottom flask. The solution was evaporated *in vacuo* to an oily orange residue which was then brought into the glovebox and dissolved in minimal (~2 mL) of toluene, layered with ~5 mL hexanes and then placed in the freezer. After 4 days, a crop of orange-yellow crystals was produced. The supernatant was decanted, and the solids washed with 3 x 1 mL hexanes. The precipitate was then dissolved in benzene and evaporated to dryness to liberate trapped toluene and dried *in vacuo* for 3 hours, yielding $[(AS_2^{Ph2})_2ThCl_2]$ (**1**) as a yellow-orange solid in 29 % yield (50.8 mg). X-ray quality crystals of $[(AS_2^{Ph2})_2ThCl_2]$·2 hexanes (**1·2 hexanes**) were grown from an *o*-difluorobenzene solution layered with hexanes cooled to –30 °C for one week. **^1H NMR** (C_6D_6, 600 MHz): δ 7.49 (s, 2H, AcridanC*H*), 7.29 (s, 2H, AcridanC*H*), 7.27–7.26 (d, $J_{H–H}$ 6.21 Hz, 4H, *o*-Ph), 7.06–7.04 (m, 4H, *o*-Ph), 7.04 (s, 2H, AcridanC*H*), 6.70 (s, 2H, AcridanC*H*), 6.69–6.65 (m, 6H, *m*,*p*-Ph), 6.61–6.58 (m, 6H, *m*,*p*-Ph), 2.14 (s, 6H, C*Me*), 2.03 (s, 6H, C*Me*), 1.84 (s, 6H, CMe_2), 1.83 (s, 6H, CMe_2). **$^{13}C\{^1H\}$ NMR** (C_6D_6, 150 MHz): δ 151.32 (Acridan*C*Se), 150.16 (Acridan*C*Se), 136.15 (Ph*C*Se), 136.00 (Acridan*C*H), 135.27 (Acridan*C*), 135.12 (Ph*C*Se), 133.57 (Acridan*C*), 132.22 (*o*-Ph), 130.74 (*C*Me), 130.27 (*C*Me), 129.94 (*o*-Ph/Acridan*C*H), 128.95 (*m*,*p*-Ph), 128.81 (*m*,*p*-Ph), 127.04 (2 x *m*,*p*-Ph), 126.93 (Acridan*C*H), 126.80 (Acridan*C*H), 120.56 (Acridan*C*N), 112.92 (Acridan*C*N), 37.62 (CMe_2), 33.03 (C*Me*), 25.36 (CMe), 20.74 (2 x CMe_2). **Anal. Calcd.** ($C_{58}H_{52}Cl_2N_2S_4Th$): C, 57.66; H, 4.34; N, 2.32. **Found:** C, 57.86; H, 4.83; N, 2.29 %.

$[(ASe_2^{Ph2})_2ThCl_2]$ (2): In the glovebox, $ThCl_4(dme)_2$ (80.0 mg, 0.144 mmol) and $[\{Li(ASe_2^{Ph2})\}_2]$ (160 mg, 0.289 mmol) were charged to a 20

mL scintillation vial, dissolved in ~8 mL of toluene and stirred for 30 minutes. ~1 mL of hexanes was added to the solution, which was allowed to stir for another 5 minutes, after which, the orange solution was filtered through a small celite plug to remove LiCl and collected in a 25 mL round-bottom flask. The solution was evaporated *in vacuo* to an oily orange residue which was then brought into the glovebox and dissolved in minimal (~3 mL) of Et_2O, layered with ~15 mL hexanes and then placed in the freezer. After 1 day, a crop of orange-yellow crystals was produced. The supernatant was decanted, and the solids washed with 2 x 1 mL hexanes. The precipitate was then dried *in vacuo* for 1 hour, yielding $[(ASe_2^{Ph2})_2ThCl_2]$ (**2**) as a yellow-orange solid in 40 % yield (80.4 mg). X-ray quality crystals of $[(ASe_2^{Ph2})_2ThCl_2]$·toluene (**2·toluene**) were grown from a toluene solution layered with hexanes cooled to –30 °C for two weeks. **^{1}H NMR** (C_6D_6, 600 MHz): δ 7.56–7.55 (d, $J_{H–H}$ 7.06 Hz, 4H, *o*-Ph), 7.51 (s, 2H, Acridan*CH*), 7.24–7.23 (m, 4H, *o*-Ph), 7.21 (s, 2H, Acridan*CH*), 6.93 (s, 2H, Acridan*CH*), 6.90 (s, 2H, Acridan*CH*), 6.79–6.74 (m, 12H, (2 x *m*,*p*-Ph), 2.24 (s, 6H, C*Me*), 2.02 (s, 6H, C*Me*), 1.95 (s, 6H, C*Me*$_2$), 1.84 (s, 6H, C*Me*$_2$). **^{13}C{^{1}H} NMR** (C_6D_6, 150 MHz): δ 151.72 (Acridan*C*Se), 150.75 (Acridan*C*Se), 136.37 (Acridan*C*H), 135.51 (Acridan*C*), 133.73 (Acridan*C*), 132.51 (*o*-Ph), 131.48 (Ph*C*Se), 131.07 (*C*Me), 130.94 (Acridan*C*H), 130.57 (*C*Me), 130.31 (*m*,*p*-Ph), 129.66 (2 x *m*,*p*-Ph), 129.36 (Ph*C*Se), 129.24 (Acridan*C*H), 128.92 (*o*-Ph), 127.60 (*m*,*p*-Ph), 125.42 (Acridan*C*H), 120.53 (Acridan*C*N), 113.27 (Acridan*C*N), 37.82 (*C*Me$_2$), 31.76 (C*Me*$_2$), 25.04 (C*Me*$_2$), 20.83 (C*Me*), 20.80 (C*Me*). **^{77}Se{^{1}H} NMR** (C_6D_6, 114 MHz): δ 392.78 (s), 347.96 (s). **Anal. Calcd.** ($C_{58}H_{52}Cl_2N_2Se_4Th$): C, 49.91; H, 3.75; N, 2.01. **Found:** C, 50.43; H, 3.45; N, 2.13 %.

$[(ASe_2^{Ph2})_2UCl_2]$ (3): In the glovebox, UCl_4 (50.0 mg, 0.132 mmol) and $[\{Li(ASe_2^{Ph2})\}_2]$ (145.5 mg, 0.132 mmol) were charged to a 20 ml scintillation vial with a stir bar. The solids were dissolved in ~3 ml of THF and stirred. After 20 minutes ~1 ml of hexanes was added to the dark brown solution and the reaction was allowed to stir for an additional 5 minutes before filtering the supernatant through a celite plug to remove LiCl. The dark brown solution was collected in a 25 ml round-bottom flask and dried *in vacuo*, leaving a black residue. The flask was brought back into the glovebox and the residue was taken up in 1-2 ml of Et_2O, which was then layered with ~16 ml hexanes and placed in a –30 °C freezer to recrystallize overnight. The dark brown supernatant was decanted and the remaining solid washed with 2 x 1 ml hexanes. The precipitate was dried *in vacuo* for 1 hour and brought back into the glovebox. 60.2 mg of dark brown $[(ASe_2^{Ph2})_2UCl_2]$ (**3**) was collected in 33% yield. X-ray quality crystals of $[(ASe_2^{Ph2})_2UCl_2]$·toluene (**3·toluene**) were grown from a toluene solution layered with hexanes cooled to –30 °C for one week. **^{1}H NMR** (C_6D_6, 600 MHz): δ 22.17 (s, 2H), 19.12 (s, 6H, C*H*$_3$), 15.52 (s, 2H), 9.85 (s, 6H, C*H*$_3$), 8.55 (s, 6H, C*H*$_3$), 7.69 (s, 2H), 7.61 (br s, 4H, *o*,*m*-Ph), 7.55 (br s, 4H, *o*,*m*-Ph), 7.09 (br s, 2H), 0.45 (br s, 2H), –0.55 (s, 4H, *o*,*m*-Ph), –3.35 (s, 6H, C*H*$_3$), –6.66 (s, 4H, *o*,*m*-Ph), –14.06 (s, 2H). **Anal. Calcd.** ($C_{58}H_{52}Cl_2N_2Se_4U$): C, 49.69; H, 3.74; N, 2.00%. **Found:** C, 49.17; H, 4.13; N, 2.03 %.

FOOTNOTES

† CSD version 5.45, updated June 2024.

‡ In **1**, each ligand features nine inter-ring C···C distances below 4.0 Å, and the shortest C···C distance for the two ligands is 3.510 or 3.518 Å; in **2**, five C···C distances are below 4.0 Å, and the shortest distance is 3.633 Å; in **3**, three C···C distances are below 4.0 Å, and the shortest distance is 3.585 Å.[74]

§ Compounds **1**–**3** were formed as the major reaction product, and the low yields are attributed to losses during recrystallization. Attempts to prepare a uranium analogue of compound **1** were not undertaken.

ASSOCIATED CONTENT

Supporting Information

The Supporting Information is available free of charge on the ACS Publications website. NMR spectra, computational data, SHAPE analysis (PDF). DFT Structures (XYZ).

Accession Codes

CCDC 2371737–2371739 contain the supplementary crystallographic data for compounds **1**–**3**, respectively. These data can be obtained free of charge via www.ccdc.cam.ac.uk/data_request/cif, or by emailing data_request@ccdc.cam.ac.uk, or by contacting The Cambridge Crystallographic Data Centre, 12 Union Road, Cambridge CB2 1EZ, UK; fax: +44 1223 336033.

AUTHOR INFORMATION

Corresponding Author

* David J. H. Emslie − *Department of Chemistry and Chemical Biology, McMaster University, Hamilton, Ontario, Canada, L8S 4M1; orcid.org/0000-0002-2570-9345*
Email: emslied@mcmaster.ca

Author

Novan A. G. Gray − *Department of Chemistry and Chemical Biology, McMaster University, Hamilton, Ontario, Canada, L8S 4M1; orcid.org/0000-0003-3607-4063*

ACKNOWLEDGMENT

D.J.H.E. thanks NSERC of Canada for a Discovery Grant and the Digital Research Alliance of Canada (previously Compute Canada) for a 2020 Resources for Research Groups (RRG) grant. N.A.G.G. thanks the Government of Ontario for an Ontario Graduate Scholarship (OGS). We are also grateful to Dr. Jeffrey S. Price for helpful crystallographic discussions and Dr. Ignacio Vargas-Baca for helpful discussions on quantum chemical calculations. This paper is dedicated to Dr. James F. Britten on the occasion of his retirement.

REFERENCES

(1) Leoncini, A.; Huskens, J.; Verboom, W. Ligands for f-element extraction used in the nuclear fuel cycle, *Chem. Soc. Rev.* **2017**, *46*, 7229-7273.

(2) Lehman-Andino, I.; Su, J.; Papathanasiou, K. E.; Eaton, T. M.; Jian, J.; Dan, D.; Albrecht-Schmitt, T. E.; Dares, C. J.; Batista, E. R.; Yang, P.; Gibson, J. K.; Kavallieratos, K. Soft-donor dipicolinamide derivatives for selective actinide(III)/lanthanide(III) separation: the role of S- vs. O-donor sites, *Chem. Commun.* **2019**, *55*, 2441-2444.

(3) Bessen, N. P.; Jackson, J. A.; Jensen, M. P.; Shafer, J. C. Sulfur donating extractants for the separation of trivalent actinides and lanthanides, *Coord. Chem. Rev.* **2020**, *421*, 213446.

(4) Bessen, N.; Yan, Q.; Pu, N.; Chen, J.; Xu, C.; Shafer, J. Extraction of the trivalent transplutonium actinides americium through einsteinium by the sulfur donor Cyanex 301, *Inorg. Chem. Front.* **2021**, *8*, 4177-4185.

(5) Klaehn, J. R.; Peterman, D. R.; Harrup, M. K.; Tillotson, R. D.; Luther, T. A.; Law, J. D.; Daniels, L. M. Synthesis of symmetric dithiophosphinic acids for "minor actinide" extraction, *Inorg. Chim. Acta* **2008**, *361*, 2522-2532.

(6) Zalupski, P. R.; Klaehn, J. R.; Peterman, D. R. Complete Recovery of Actinides from UREX-like Raffinates Using a Combination of Hard and Soft Donor Ligands. II. Soft Donor Structure Variation, *Solvent Extr. Ion Exc.* **2015**, *33*, 523-539.

(7) Neidig, M. L.; Clark, D. L.; Martin, R. L. Covalency in f-element complexes, *Coord. Chem. Rev.* **2013**, *257*, 394-406.

(8) Ephritikhine, M. Molecular actinide compounds with soft chalcogen ligands, *Coord. Chem. Rev.* **2016**, *319*, 35-62.

(9) Behrle, A. C.; Barnes, C. L.; Kaltsoyannis, N.; Walensky, J. R. Systematic Investigation of Thorium(IV)– and Uranium(IV)–Ligand Bonding in Dithiophosphonate, Thioselenophosphinate, and Diselenophosphonate Complexes, *Inorg. Chem.* **2013**, *52*, 10623-10631.

(10) Behrle, A. C.; Kerridge, A.; Walensky, J. R. Dithio- and Diselenophosphinate Thorium(IV) and Uranium(IV) Complexes: Molecular and Electronic Structures, Spectroscopy, and Transmetalation Reactivity, *Inorg. Chem.* **2015**, *54*, 11625-11636.

(11) Jones, M. B.; Gaunt, A. J.; Gordon, J. C.; Kaltsoyannis, N.; Neu, M. P.; Scott, B. L. Uncovering f-element bonding differences and electronic structure in a series of 1 : 3 and 1 : 4 complexes with a diselenophosphinate ligand, *Chem. Sci.* **2013**, *4*, 1189-1203.

(12) Karaghiosoff, K.; Klapötke, T. M.; Kunz, T.; Mayer, P.; Beck, W. Uranyl Complexes with Selenium or Tellurium Containing Chelate Ligands, *Z. Anorg. Allg. Chem.* **2021**, *647*, 943-950.

(13) Goodwin, C. A. P.; Janicke, M. T.; Scott, B. L.; Gaunt, A. J. $[AnI_3(THF)_4]$ (An = Np, Pu) Preparation Bypassing An^0 Metal Precursors: Access to Np^{3+}/Pu^{3+} Nonaqueous and Organometallic Complexes, *J. Am. Chem. Sci.* **2021**, *143*, 20680-20696.

(14) Goodwin, C. A. P.; Schlimgen, A. W.; Albrecht-Schönzart, T. E.; Batista, E. R.; Gaunt, A. J.; Janicke, M. T.; Kozimor, S. A.; Scott, B. L.; Stevens, L. M.; White, F. D.; Yang, P. Structural and Spectroscopic Comparison of Soft-Se vs. Hard-O Donor Bonding in Trivalent Americium/Neodymium Molecules, *Angew. Chem. Int. Ed.* **2021**, *60*, 9459-9466.

(15) Gaunt, A. J.; Reilly, S. D.; Enriquez, A. E.; Scott, B. L.; Ibers, J. A.; Sekar, P.; Ingram, K. I. M.; Kaltsoyannis, N.; Neu, M. P. Experimental and Theoretical Comparison of Actinide and Lanthanide Bonding in $M[N(EPR_2)_2]_3$ Complexes (M = U, Pu, La, Ce; E = S, Se, Te; R = Ph, ^{i}Pr, H), *Inorg. Chem.* **2008**, *47*, 29-41.

(16) Gaunt, A. J.; Scott, B. L.; Neu, M. P. Homoleptic uranium(III) imidodiphosphinochalcogenides including the first structurally characterised molecular trivalent actinide–Se bond, *Chem. Commun.* **2005**, 3215-3217.

(17) Gaunt, A. J.; Scott, B. L.; Neu, M. P. A Molecular Actinide–Tellurium Bond and Comparison of Bonding in $[M^{III}\{N(TeP^iPr_2)_2\}_3]$ (M=U, La), *Angew. Chem. Int. Ed.* **2006**, *45*, 1638-1641.

(18) Zalkin, A.; Brennan, J. G. A trivalent-uranium thioether coordination compound, *Acta Crystallogr., Sect. C: Cryst. Struct. Commun.* **1985**, *41*, 1295-1297.

(19) Shinomoto, R.; Zalkin, A.; Edelstein, N. M. Preparation and crystal structures of tetrakis(methyltrihydroborato)uranium(IV)bis(tetrahydrofuranate) and tetrakis(methyltrihydroborato)uranium(IV)tetrahydrothiophenate, *Inorg. Chim. Acta* **1987**, *139*, 91-95.

(20) Shinomoto, R.; Zalkin, A.; Edelstein, N. M.; Zhang, D. Preparation and crystal structures of complexes of uranium(4+) methyltrihydroborate(1-) with 1,2-dimethoxyethane, N,N,N',N'-tetramethylethylenediamine, and 1,2-bis(methylthio)ethane, *Inorg. Chem.* **1987**, *26*, 2868-2872.

(21) Karmazin, L.; Mazzanti, M.; Pécaut, J. Unique crown thioether complexes of f elements: the crystal structure of U(III) and La(III) complexes of 1,4,7-trithiacyclononane, *Chem. Commun.* **2002**, 654-655.

(22) Arliguie, T.; Belkhiri, L.; Bouaoud, S.-E.; Thuéry, P.; Villiers, C.; Boucekkine, A.; Ephritikhine, M. Lanthanide(III) and Actinide(III) Complexes $[M(BH_4)_2(THF)_5][BPh_4]$ and $[M(BH_4)_2$(18-crown-6)$][BPh_4]$ (M = Nd, Ce, U): Synthesis, Crystal Structure, and Density Functional Theory Investigation of the Covalent Contribution to Metal-Borohydride Bonding, *Inorg. Chem.* **2009**, *48*, 221-230.

(23) Baracco, L.; Bombieri, G.; Degetto, S.; Forsellini, E.; Marangoni, G.; Paolucci, G.; Graziani, R. Preparation, characterization, and crystal structure of *cis*-dichloro-[*meso*-bis(*trans*-2-hydroxycyclohexyl) sulphide-*OOS*]dioxouranium(VI), *J. Chem. Soc., Dalton Trans.* **1975**, 2161-2164.

(24) Casellato, U.; Sitran, S.; Tamburini, S.; Vigato, P. A.; Graziani, R. Preparation, properties, crystal and molecular structure of uranyl(VI) complexes with a new cyclic Schiff base compartmental ligand, *Inorg. Chim. Acta* **1986**, *114*, 111-117.

(25) Fenton, D. E.; Vigato, P. A.; Casellato, U.; Graziani, R.; Vidali, M. The preparation and crystal structure of N,N′-bis(salicylidene)-1,5-diamino-3-thiapentane-dioxouranium(VI), *Inorg. Chim. Acta* **1981**, *51*, 195-199.

(26) Sitran, S.; Fregona, D.; Casellato, U.; Vigato, P. A.; Graziani, R.; Faraglia, G. Dioxouranium(Vl) complexes with pentadentate bases containing acetal groups, *Inorg. Chim. Acta* **1987**, *132*, 279-288.

(27) Takeyama, T.; Takao, K. Effects of coordinating heteroatoms on molecular structure, thermodynamic stability and redox behavior of uranyl(VI) complexes with pentadentate Schiff-base ligands, *RSC Adv.* **2022**, *12*, 24260-24268.

(28) Gray, N. A. G.; Price, J. S.; Emslie, D. J. H. Uranium(IV) Thio- and Selenoether Complexes: Syntheses, Structures, and Computational Investigation of U−ER_2 Interactions, *Chem. − Eur. J.* **2022**, *28*, e202103580.

(29) Vidjayacoumar, B.; Ilango, S.; Ray, M. J.; Chu, T.; Kolpin, K. B.; Andreychuk, N. R.; Cruz, C. A.; Emslie, D. J. H.; Jenkins, H. A.; Britten, J. F. Rigid NON- and NSN-ligand complexes of tetravalent and trivalent uranium: comparison of U–OAr_2 and U–SAr_2 bonding, *Dalton Trans.* **2012**, *41*, 8175-8189.

(30) Barnea, E.; Andrea, T.; Kapon, M.; Eisen, M. S. Formation of Inclusion Organoactinide Complexes with Boron-Containing Macrocycles, *J. Am. Chem. Sci.* **2004**, *126*, 5066-5067.

(31) Gaunt, A. J.; Matonic, J. H.; Scott, B. L.; Neu, M. P., 5f Element Complexes with 'Soft' Donor Atom Ligands: Eight Coordinate Pu(III) Pyrazinyl and Thioether Complexes. In *Recent Advances in Actinide Science*, May, I.; Bryan, N. D.; Alvares, R., Eds.; The Royal Society of Chemistry: 2006; p 183-185.

(32) Behrle, A. C.; Levin, J. R.; Kim, J. E.; Drewett, J. M.; Barnes, C. L.; Schelter, E. J.; Walensky, J. R. Stabilization of M^{IV} = Ti, Zr, Hf, Ce, and Th using a selenium bis(phenolate) ligand, *Dalton Trans.* **2015**, *44*, 2693-2702.

(33) Myers, A. J.; Rungthanaphatsophon, P.; Behrle, A. C.; Vilanova, S. P.; Kelley, S. P.; Lukens, W. W.; Walensky, J. R. Structure and properties of $[(4,6\text{-}^tBu_2C_6H_2O)_2Se]_2An(THF)_2$, An = U, Np, and their reaction with *p*-benzoquinone, *Chem. Commun.* **2018**, *54*, 10435-10438.

(34) Spencer, L. P.; Yang, P.; Scott, B. L.; Batista, E. R.; Boncella, J. M. Oxidative Addition to U(V)−U(V) Dimers: Facile Routes to Uranium(VI) Bis(imido) Complexes, *Inorg. Chem.* **2009**, *48*, 11615-11623.

(35) Franke, S. M.; Heinemann, F. W.; Meyer, K. Reactivity of uranium(IV) bridged chalcogenido complexes U^{IV}–E–U^{IV} (E = S, Se) with elemental sulfur and selenium: synthesis of polychalcogenido-bridged uranium complexes, *Chem. Sci.* **2014**, *5*, 942-950.

(36) Gray, N. A. G.; Vargas-Baca, I.; Emslie, D. J. H. A Synthetic, Structural, Spectroscopic, and Computational Study of Alkali Metal–Thioether, −Selenoether, and −Telluroether Interactions, *Inorg. Chem.* **2023**, *62*, 16974-16985.

(37) Sluis, P. v. d.; Spek, A. L. BYPASS: An effective method for the refinement of crystal structures containing disordered solvent regions, *Acta Crystallogr., Sect. A: Found. Crystallogr.* **1990**, *46*, 194-201.

(38) Cordero, B.; Gómez, V.; Platero-Prats, A. E.; Revés, M.; Echeverría, J.; Cremades, E.; Barragán, F.; Alvarez, S. Covalent radii revisited, *Dalton Trans.* **2008**, 2832-2838.

(39) Shannon, R. Revised effective ionic radii and systematic studies of interatomic distances in halides and chalcogenides, *Acta Crystallogr., Sect. A: Found. Crystallogr.* **1976**, *32*, 751-767.

(40) Cremer, D.; Kraka, E. A description of the chemical bond in terms of local properties of electron density and energy, *Croat. Chem. Acta* **1984**, *57*, 1259-1281.

(41) Cremer, D.; Kraka, E. Chemical Bonds without Bonding Electron Density — Does the Difference Electron-Density Analysis Suffice for a Description of the Chemical Bond?, *Angew. Chem. Int. Ed.* **1984**, *23*, 627-628.

(42) Cantat, T.; Scott, B. L.; Kiplinger, J. L. Convenient access to the anhydrous thorium tetrachloride complexes $ThCl_4(DME)_2$, $ThCl_4(1,4\text{-dioxane})_2$ and $ThCl_4(THF)_{3.5}$ using commercially available and inexpensive starting materials, *Chem. Commun.* **2010**, *46*, 919-921.

(43) Kiplinger, J. L.; Morris, D. E.; Scott, B. L.; Burns, C. J. Convenient Synthesis, Structure, and Reactivity of $(C_5Me_5)U(CH_2C_6H_5)_3$: A Simple Strategy for the Preparation of Monopentamethylcyclopentadienyl Uranium(IV) Complexes, *Organometallics* **2002**, *21*, 5978-5982.

(44) Harris, R. K.; Becker, E. D.; Cabral De Menezes, S. M.; Goodfellow, R.; Granger, P. NMR nomenclature: Nuclear spin properties and conventions for chemical shifts (IUPAC recommendations 2001), *Concepts Magn. Reson.* **2002**, *14*, 326-346.

(45) Sheldrick, G. SHELXT - Integrated space-group and crystal-structure determination, *Acta Crystallogr., Sect. A: Found. Crystallogr.* **2015**, *71*, 3-8.

(46) Sheldrick, G. Crystal structure refinement with SHELXL, *Acta Crystallogr., Sect. C: Cryst. Struct. Commun.* **2015**, *71*, 3-8.

(47) Dolomanov, O. V.; Bourhis, L. J.; Gildea, R. J.; Howard, J. A. K.; Puschmann, H. OLEX2: a complete structure solution, refinement and analysis program, *J. Appl. Crystallogr.* **2009**, *42*, 339-341.

(48) te Velde, G.; Bickelhaupt, F. M.; Baerends, E. J.; Fonseca Guerra, C.; van Gisbergen, S. J. A.; Snijders, J. G.; Ziegler, T. Chemistry with ADF, *J. Comput. Chem.* **2001**, *22*, 931-967.

(49) Fonseca Guerra, C.; Snijders, J. G.; te Velde, G.; Baerends, E. J. Towards an order-N DFT method, *Theor. Chem. Acc.* **1998**, *99*, 391-403.

(50) ADF 2023, SCM., *Theoretical Chemistry*, Vrije Universiteit Amsterdam, The Netherlands, http://www.scm.com.

(51) Perdew, J. P.; Burke, K.; Ernzerhof, M. Generalized Gradient Approximation Made Simple, *Phys. Rev. Lett.* **1996**, *77*, 3865-3868.

(52) van Lenthe, E.; Ehlers, A.; Baerends, E.-J. Geometry optimizations in the zero order regular approximation for relativistic effects, *J. Chem. Phys.* **1999**, *110*, 8943-8953.

(53) van Lenthe, E.; van Leeuwen, R.; Baerends, E. J.; Snijders, J. G. Relativistic regular two-component Hamiltonians, *Int. J. Quantum Chem.* **1996**, *57*, 281-293.

(54) Lenthe, E. v.; Baerends, E. J.; Snijders, J. G. Relativistic regular two-component Hamiltonians, *J. Chem. Phys.* **1993**, *99*, 4597-4610.

(55) van Lenthe, E.; Baerends, E. J.; Snijders, J. G. Relativistic total energy using regular approximations, *J. Chem. Phys.* **1994**, *101*, 9783-9792.

(56) van Lenthe, E.; Snijders, J. G.; Baerends, E. J. The zero-order regular approximation for relativistic effects: The effect of spin–orbit coupling in closed shell molecules, *J. Chem. Phys.* **1996**, *105*, 6505-6516.

(57) Grimme, S.; Antony, J.; Ehrlich, S.; Krieg, H. A consistent and accurate ab initio parametrization of density functional dispersion correction (DFT-D) for the 94 elements H-Pu, *J. Chem. Phys.* **2010**, *132*, 154104.

(58) Grimme, S.; Ehrlich, S.; Goerigk, L. Effect of the damping function in dispersion corrected density functional theory, *J. Comput. Chem.* **2011**, *32*, 1456-1465.

(59) Franchini, M.; Philipsen, P. H. T.; Visscher, L. The Becke Fuzzy Cells Integration Scheme in the Amsterdam Density Functional Program Suite, *J. Comput. Chem.* **2013**, *34*, 1819-1827.

(60) Becke, A. D. A multicenter numerical integration scheme for polyatomic molecules, *J. Chem. Phys.* **1988**, *88*, 2547-2553.

(61) Jacobsen, H.; Bérces, A.; Swerhone, D. P.; Ziegler, T. Analytic second derivatives of molecular energies: a density functional implementation, *Comput. Phys. Commun.* **1997**, *100*, 263-276.

(62) Wolff, S. K. Analytical second derivatives in the Amsterdam density functional package, *Int. J. Quantum Chem.* **2005**, *104*, 645-659.

(63) Bérces, A.; Dickson, R. M.; Fan, L.; Jacobsen, H.; Swerhone, D.; Ziegler, T. An implementation of the coupled perturbed Kohn-Sham equations: perturbation due to nuclear displacements, *Comput. Phys. Commun.* **1997**, *100*, 247-262.

(64) Bader, R. F. W., *Atoms in Molecules: A Quantum Theory*, Clarendon Press: Oxford, 1990.

(65) Rodríguez, J. I.; Köster, A. M.; Ayers, P. W.; Santos-Valle, A.; Vela, A.; Merino, G. An efficient grid-based scheme to compute QTAIM atomic properties without explicit calculation of zero-flux surfaces, *J. Comput. Chem.* **2009**, *30*, 1082-1092.

(66) Rodríguez, J. I. An efficient method for computing the QTAIM topology of a scalar field: The electron density case, *J. Comput. Chem.* **2013**, *34*, 681-686.

(67) Rodríguez, J. I.; Bader, R. F. W.; Ayers, P. W.; Michel, C.; Götz, A. W.; Bo, C. A high performance grid-based algorithm for computing QTAIM properties, *Chem. Phys. Lett.* **2009**, *472*, 149-152.

(68) Ayers, P. W.; Jenkins, S. Bond metallicity measures, *Comput. Theor. Chem.* **2015**, *1053*, 112-122.

(69) Tognetti, V.; Joubert, L. Density functional theory and Bader's atoms-in-molecules theory: towards a vivid dialogue, *Phys. Chem. Chem. Phys.* **2014**, *16*, 14539-14550.

(70) Abramov, Y. On the Possibility of Kinetic Energy Density Evaluation from the Experimental Electron-Density Distribution, *Acta Crystallogr., Sect. A: Found. Crystallogr.* **1997**, *53*, 264-272.

(71) Poater, J.; Solà, M.; Duran, M.; Fradera, X. The calculation of electron localization and delocalization indices at the Hartree–Fock, density functional and post-Hartree–Fock levels of theory, *Theor. Chem. Acc.* **2002**, *107*, 362-371.

(72) Fradera, X.; Austen, M. A.; Bader, R. F. W. The Lewis Model and Beyond, *J. Phys. Chem. A* **1999**, *103*, 304-314.

(73) NBO 6.0: Glendening, E. D.; Badenhoop, J. K.; Reed, A. E.; Carpenter, J. E.; Bohmann, J. A.; Morales, C. M.; Landis, C. R.; Weinhold, F., *Theoretical Chemistry Institute*, University of Wisconsin: Madison, 2013.

(74) Dance, I. Distance criteria for crystal packing analysis of supramolecular motifs, *New J. Chem.* **2003**, *27*, 22-27.

Table of Contents Graphic and Text

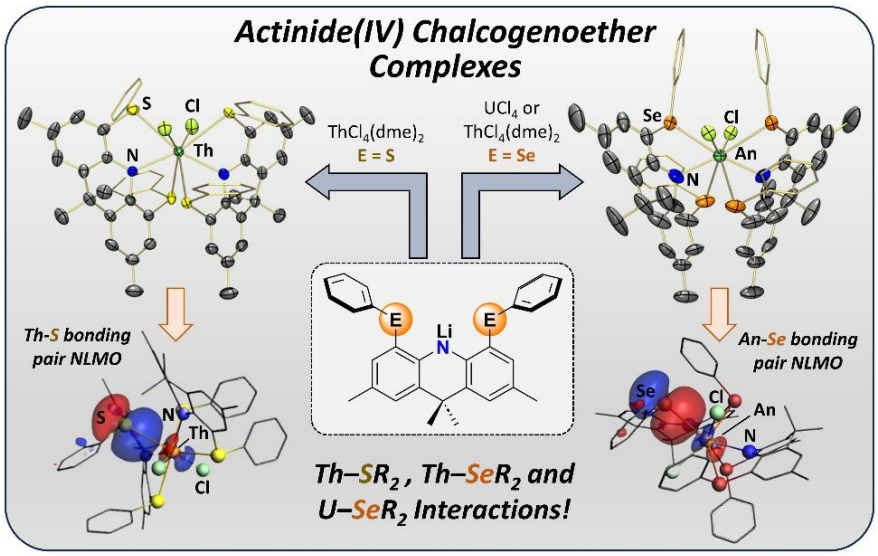

Thorium–thioether, thorium–selenoether, and uranium–selenoether complexes have been synthesized using rigid ENE-donor pincer ligands (E = S or Se), and DFT and QTAIM calculations confirm the presence of significant and partially covalent An(IV)–ER_2 interactions.